Chem, Volume *3*

Supplemental Information

Multi-functional Flexible Aqueous Sodium-Ion Batteries with High Safety

Zhaowei Guo, Yang Zhao, Yuxue Ding, Xiaoli Dong, Long Chen, Jingyu Cao, Changchun Wang, Yongyao Xia, Huisheng Peng, and Yonggang Wang

Supplemental Figures

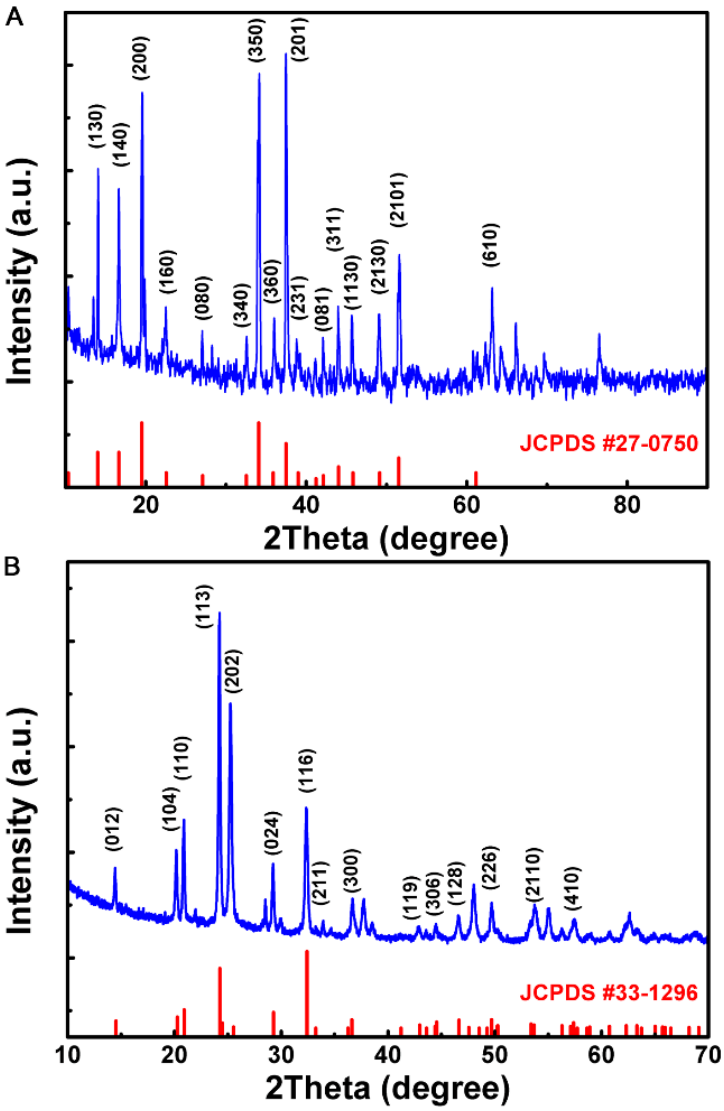

Figure S1. XRD patterns of as-prepared $Na_{0.44}MnO_2$ (A) and $NaTi_2(PO_4)_3$@C (B).

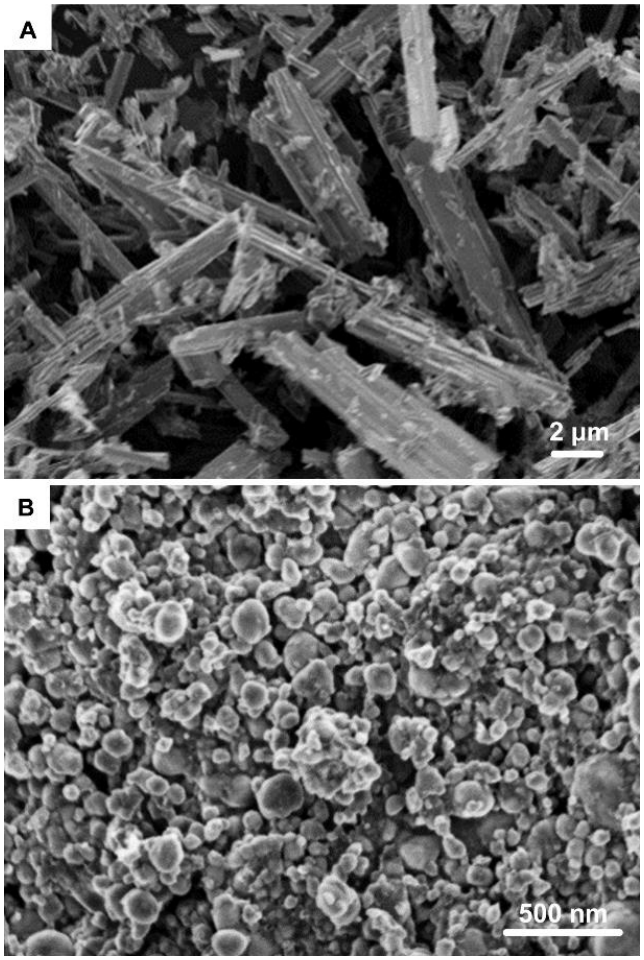

Figure S2. SEM images of as-prepared $Na_{0.44}MnO_2$ (A) and $NaTi_2(PO_4)_3$@C (B).

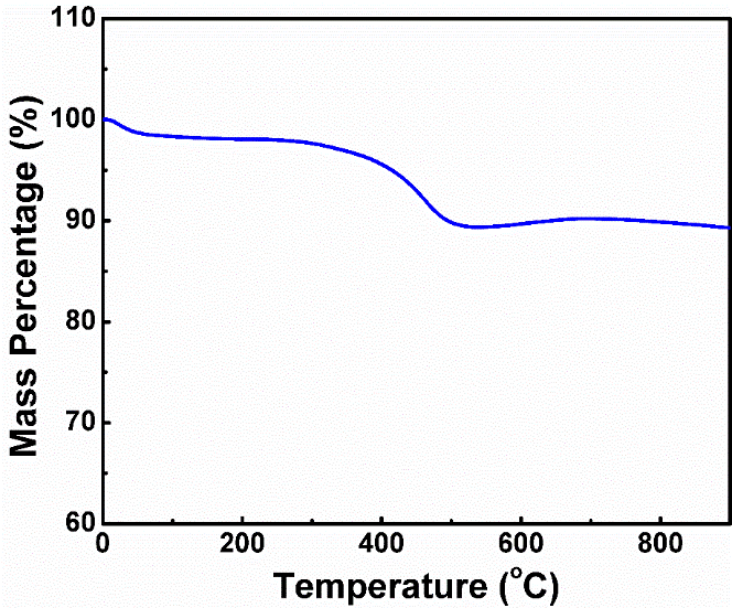

Figure S3. TGA data of as-prepared $NaTi_2(PO_4)_3$@C. TGA analysis was carried out in O_2 atmosphere at a heating rate of 10 °C min^{-1} on a TG209F1 instrument.

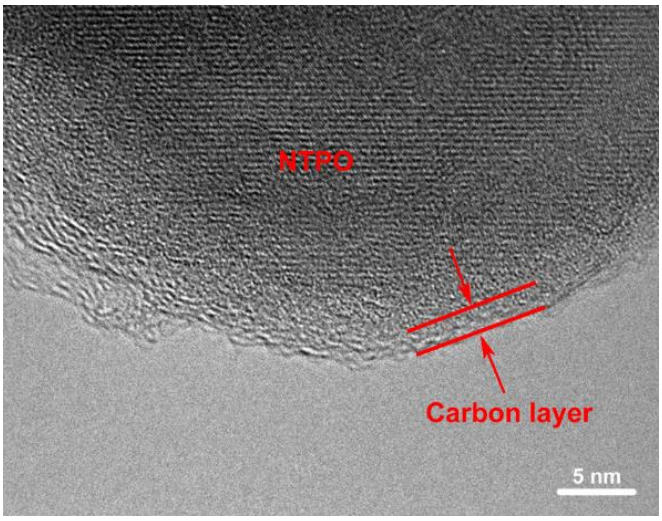

Figure S4. TEM image of as-prepared $NaTi_2(PO_4)_3$@C.

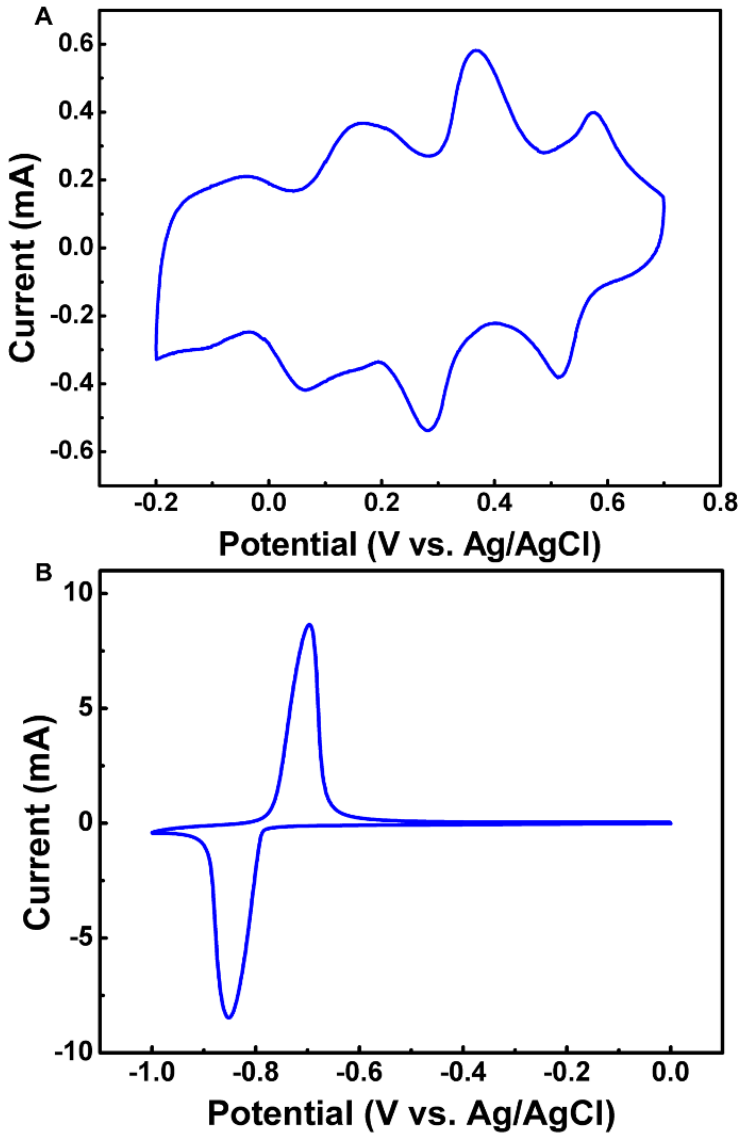

Figure S5. CV curves of $Na_{0.44}MnO_2$ electrode (A) and $NaTi_2(PO_4)_3$@C electrode (B). The cyclic voltammetry (CV) measurements of samples were carried out on CH Instruments electrochemical workstation (CHI 660D) at a scan rate of 1 mV s^{-1}. Ag/AgCl electrode (E=0.1971 V *vs.* SHE) was used as reference electrode, while activated carbon film electrode served as counter electrode. 1 M Na_2SO_4 solution was used as electrolyte.

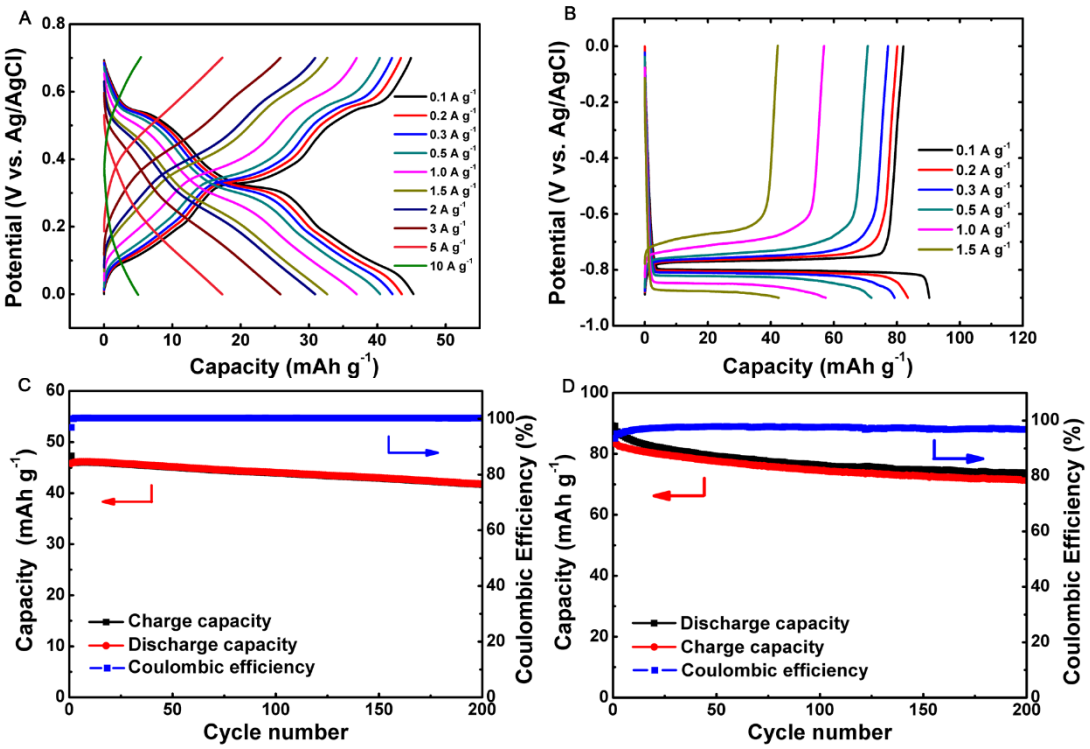

Figure S6. Electrochemical profiles of the belt-shaped $Na_{0.44}MnO_2$ film electrode and $NaTi_2(PO_4)_3$@C film electrode. (**A** and **B**) Galvanostatic charge-discharge curves of $Na_{0.44}MnO_2$ film electrode (**A**) and $NaTi_2(PO_4)_3$@C film electrode (**B**) at different current densities. (**C** and **D**) Cycling performance at the current density of 0.2 A g^{-1} of $Na_{0.44}MnO_2$ film electrode (**C**) and $NaTi_2(PO_4)_3$@C film electrode (**D**). A typical three-electrode system was used for above tests, with Ag/AgCl electrode (E=0.1971 V vs. SHE) as reference electrode, and activated carbon film electrode as counter electrode. 1 M Na_2SO_4 solution was used as electrolyte.

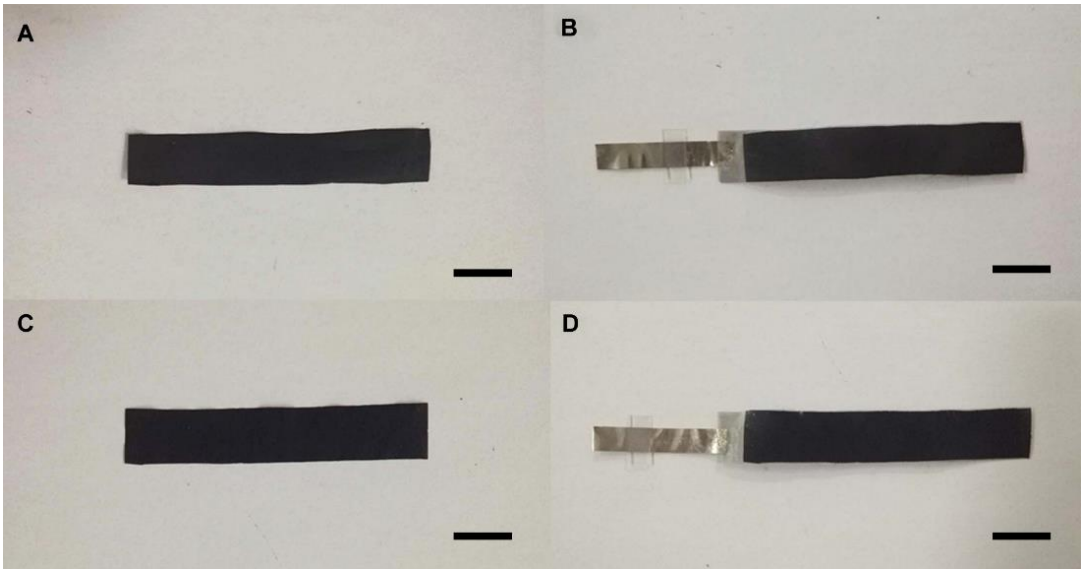

Figure S7. Photo profiles of as-prepared flexible and belt-shaped electrodes. (**A** and **B**) The mixture film ($Na_{0.44}MnO_2$ + conductive additive + binder; **A**) and the corresponding flexible and belt-shaped cathode (mixture film + current collector; **B**). (**C** and **D**) The mixture film ($NaTi_2(PO_4)_3$@C + conductive additive + binder; **C**) and the corresponding flexible and belt-shaped anode (mixture film + current collector; **D**). Scale bars: 1 cm.

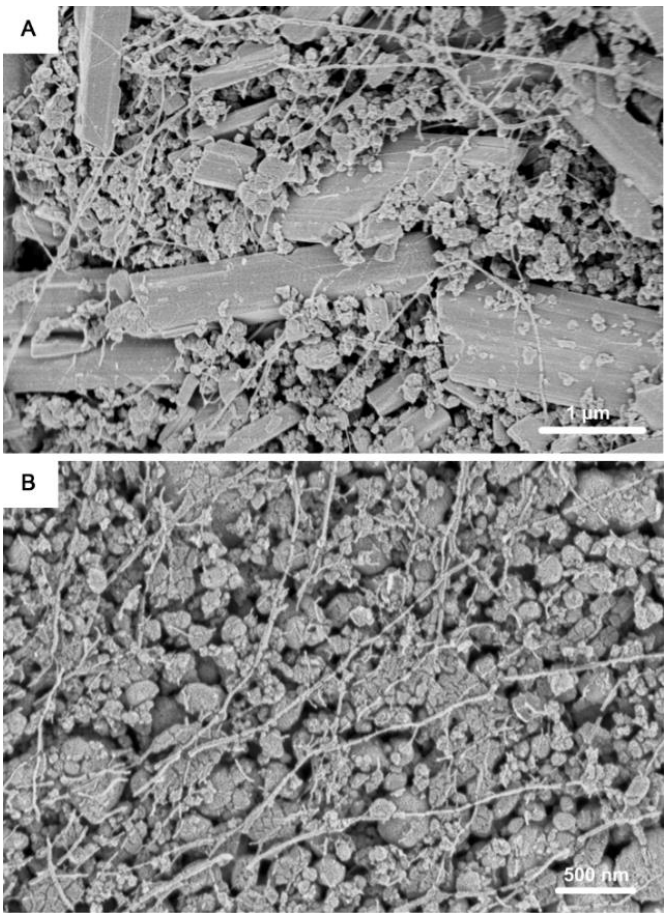

Figure S8. SEM images of flexible and belt-shaped $Na_{0.44}MnO_2$ film electrode (A) and $NaTi_2(PO_4)_3$@C film electrode (B).

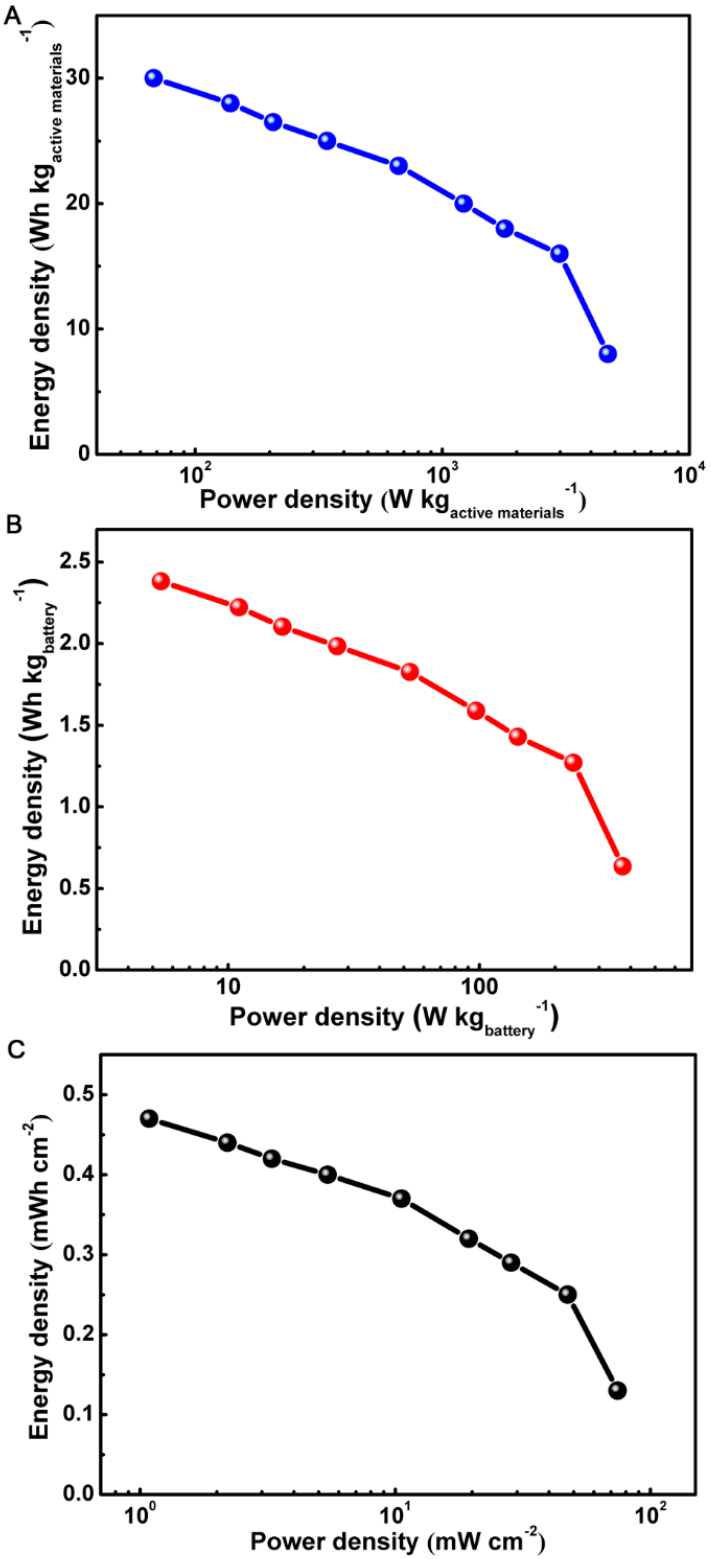

Figure S9. Ragone plot (energy density *vs.* power density) of the flexible belt-shaped $Na_{0.44}MnO_2$//$NaTi_2(PO_4)_3$@C aqueous SIB. (**A**) Mass energy/power density based on the mass loading of active materials (cathode + anode) (~79.2 mg)). (**B**) Mass energy/power density based on the total mass of the battery (~1.00 g), including active materials, current collectors, electrolyte and package and so on). (**C**) Areal energy/power density.

Figure S10. Photo profile of thickness measurement of the flexible belt-shaped $Na_{0.44}MnO_2$//$NaTi_2(PO_4)_3$@C SIB using 1 M Na_2SO_4 as electrolyte.

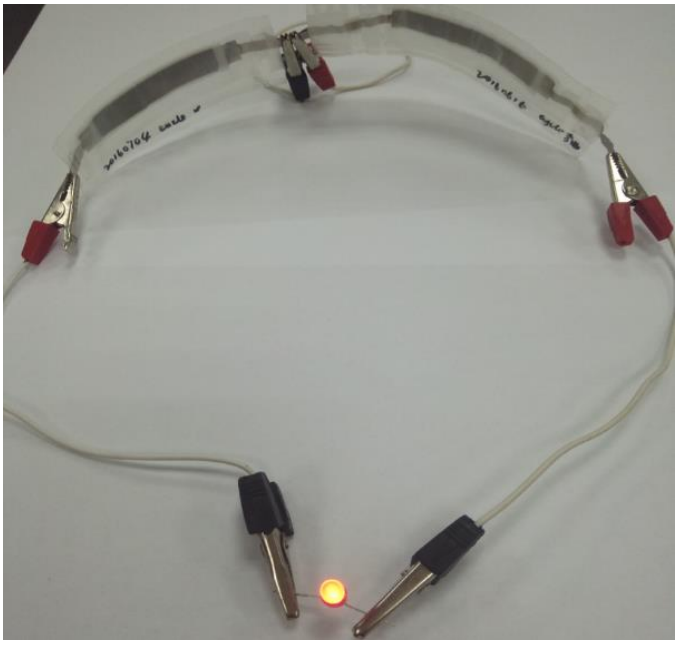

Figure S11. A red light-emitting diode (LED) powered by two flexible belt-shaped $Na_{0.44}MnO_2$//$NaTi_2(PO_4)_3$@C SIBs connected in series.

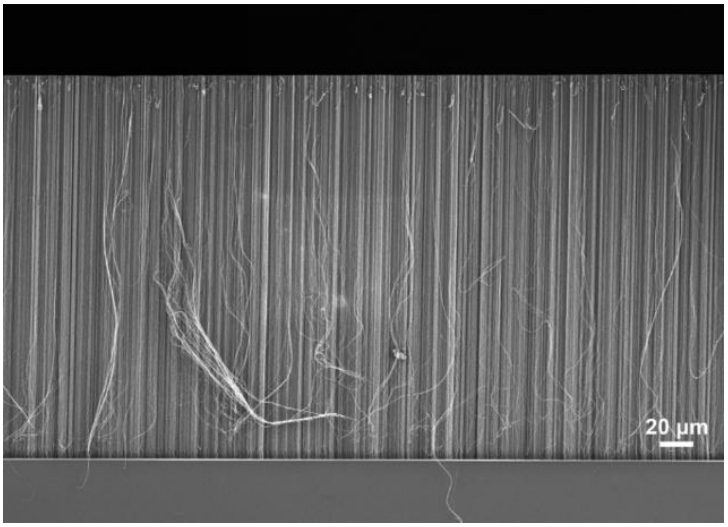

Figure S12. SEM image of a spinnable CNT array in side view.

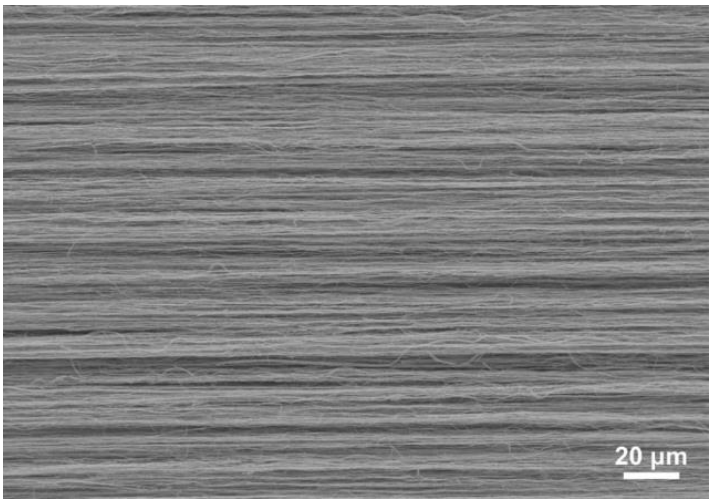

Figure S13. SEM image of the aligned CNT sheets pulled out from the spinnable CNT array.

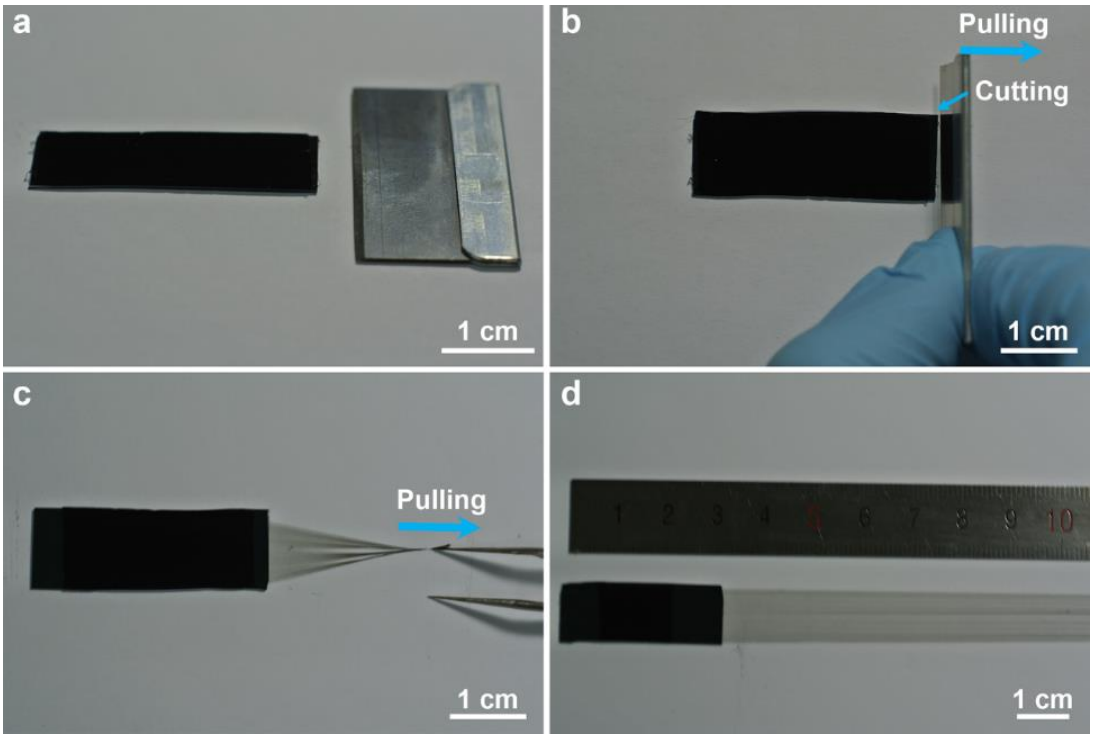

Figure S14. Photographs of the detailed preparation process of the aligned CNT sheet from a spinnable CNT array.

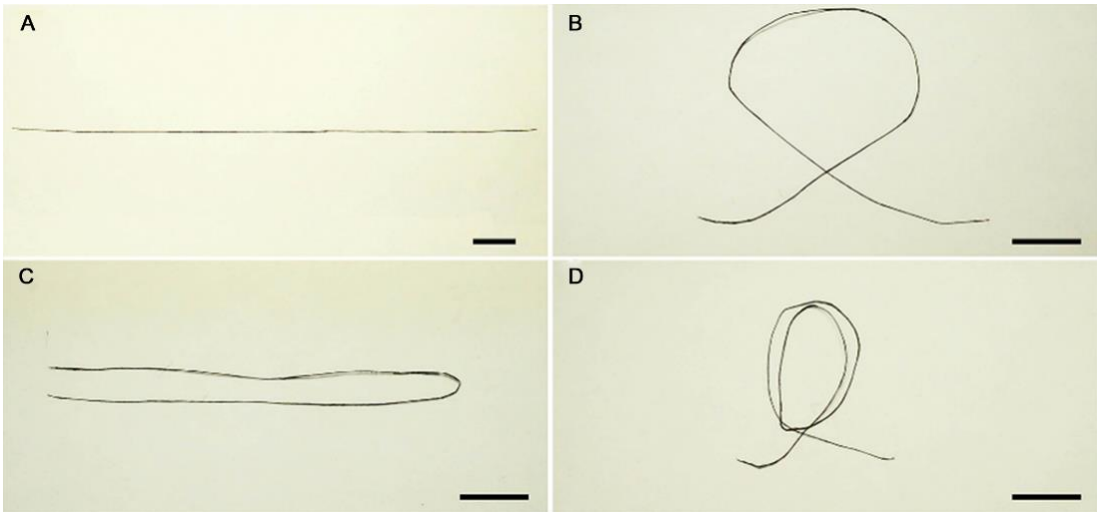

Figure S15. Photo profiles of the flexible fiber-shaped CNT based hybrid electrodes under different bending states. (**A**) Before bending. (**B**) Bended to a circle. (**C**) Bended at a degree of 180º. (**D**) Bended to two circles. Scale bars: 1 cm.

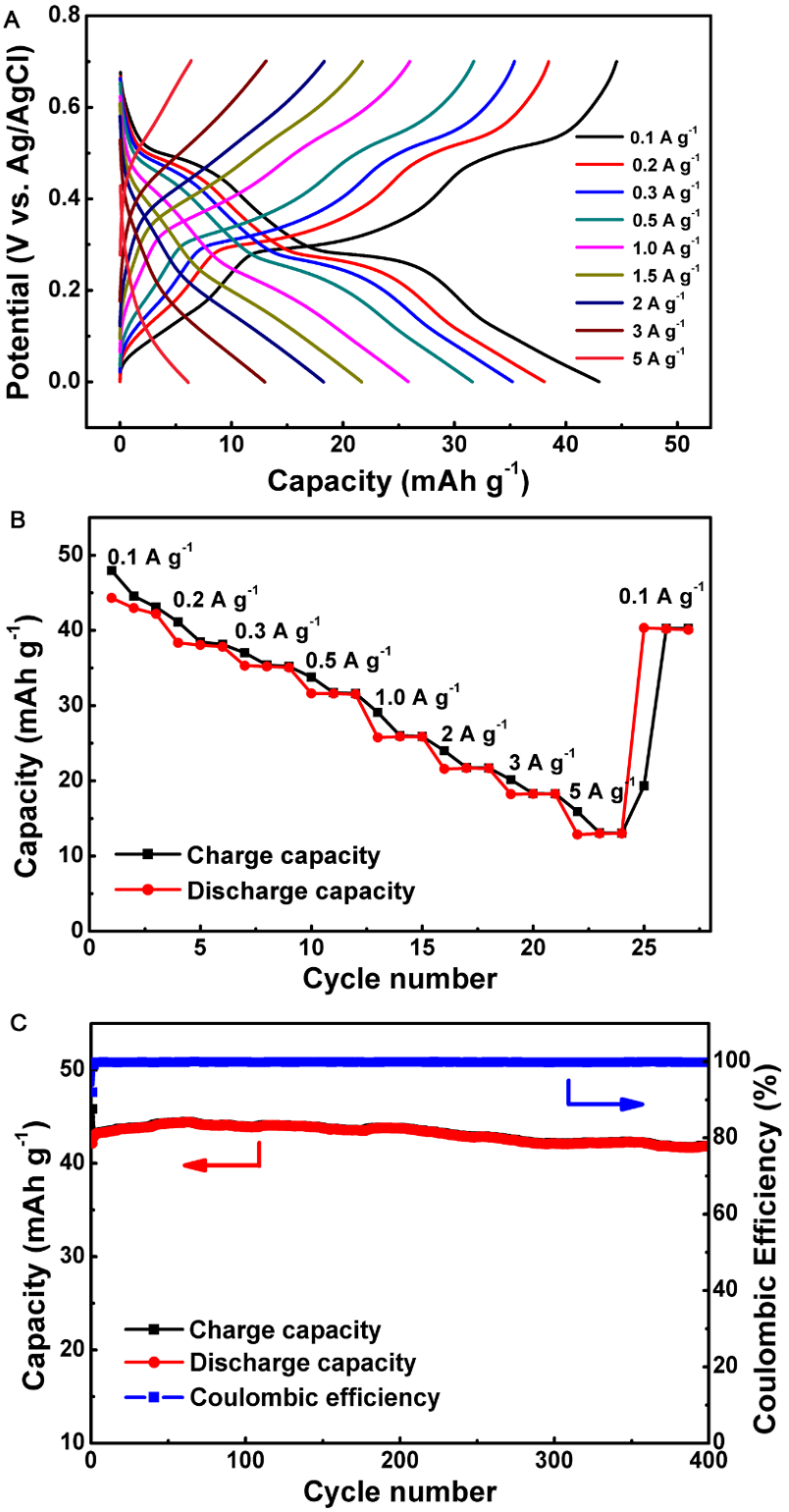

Figure S16. Electrochemical performance of flexible and fiber-shaped CNT/$Na_{0.44}MnO_2$ hybrid electrode. (**A** and **B**) Galvanostatic charge-discharge curves (**A**) and corresponding capacity stability (**B**) at different current densities. (**C**) Cycling performance at the current density of 0.2 A g^{-1}. A typical three-electrode system was used for above test, with Ag/AgCl electrode (E=0.1971 V vs. SHE) as reference electrode, and activated carbon electrode as counter electrode. 1 M Na_2SO_4 solution was used as electrolyte.

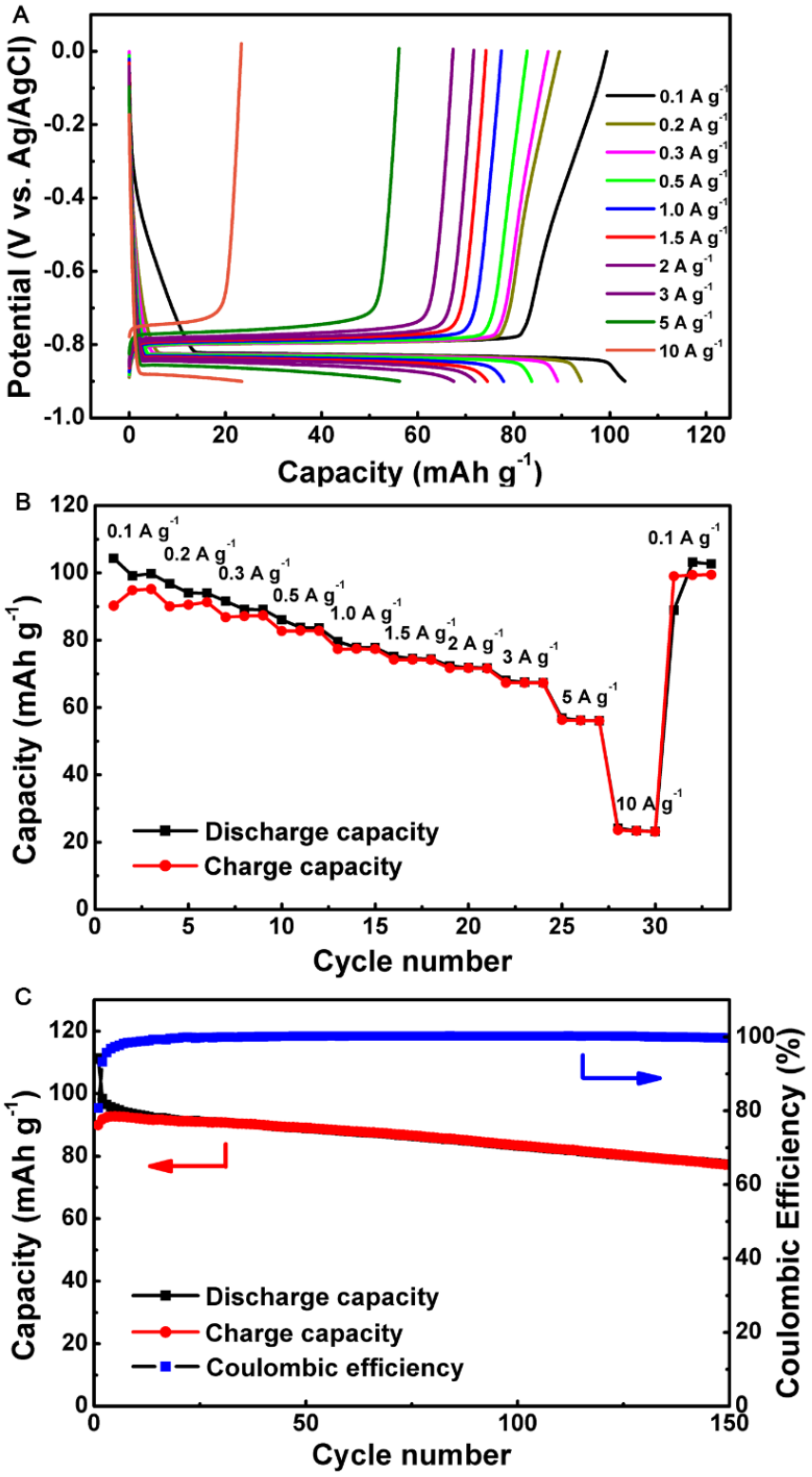

Figure S17. Electrochemical performance of flexible and fiber-shaped CNT/ $NaTi_2(PO_4)_3$@C hybrid electrode. (**A** and **B**) Galvanostatic charge-discharge curves (**A**) and corresponding capacity stability (**B**) at different current densities. (**C**) Cycling performance at the current density of 0.2 A g^{-1}. A typical three-electrode system was used for above test, with Ag/AgCl electrode (E=0.1971 V vs. SHE) as reference electrode, and activated carbon electrode as counter electrode. 1 M Na_2SO_4 solution was used as electrolyte.

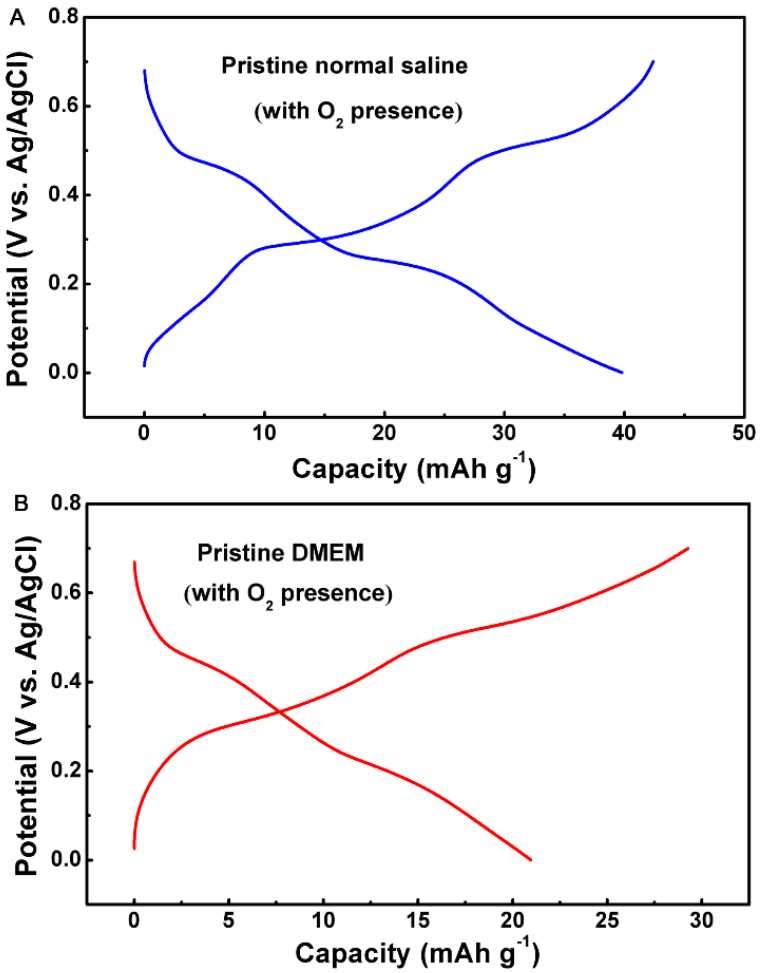

Figure S18. Galvanostatic charge-discharge curves of fiber-shaped CNT/$Na_{0.44}MnO_2$ hybrid electrode at the current density of 0.2 A g^{-1} in a pristine normal saline electrolyte solution (A) and a pristine DMEM electrolyte (B). A typical three-electrode system was used for above test, with Ag/AgCl electrode (E=0.1971 V vs. SHE) as reference electrode, and activated carbon electrode as counter electrode. 1 M Na_2SO_4 solution was used as electrolyte.

Supplemental Tables

Table S1. Comparison of electrochemical performance between present work and previous reported flexible lithium-ion batteries/supercapacitors.

Ref.	Energy Density ($mWh\ cm^{-3}$)	Power Density ($W\ cm^{-3}$)
13	0.629	0.0377
14	17.7	0.56
20	124	11.1
27	6.3	1.085
29	2.16	1.6
30	10	4
32	0.43	1.7
42	0.62	1.47
S1	3.85	0.565
S2	0.04	0.0024
S3	1.44	0.89
S4	0.61	0.85
S5	1.4	40
S6	0.55	1.391
S7	0.22	0.4
S8	0.14	0.0027
S9	6.16	0.4
S10	0.32	0.054
Present Work	**23.8**	**3.8**

NOTE: Ref. 13,14, 20, 27, 29, 30, 32 and 42 were given in the main-text. Refs. S1 to S10 are given in following Supplemental References section.

Table S2. The composition of Dulbecco's modified Eagle's medium (DMEM) used as electrolyte.

Component	Content (g/L)	Component	Content (g/L)
$CaCl_2$	0.2	L-Threonine	0.095
$Fe(NO_3)_3 \cdot 9H_2O$	0.0001	L-Tryptophan	0.016
$MgSO_4$	0.09767	L-tyrosine·2Na·$2H_2O$	0.10379
KCl	0.4	L-Valine	0.094
NaCl	6.4	Choline Chlonde	0.004
NaH_2PO_4	0.109	Folic Acid	0.004
L-Argubube·HCl	0.084	*myo*-inositol	0.0072
L-Cysteine·2HCl	0.0626	Niacinamide	0.004
L-Glutamine	0.584	D-Pantothenic Acid·$\frac{1}{2}$Ca	0.004
Glycine	0.03	Oyridoxal·HCl	0.004
L-Histidine·HCl·H_2O	0.042	Riboflavin	0.0004
L-Isoleucine	0.105	Thiamine·HCl	0.004
L-Leucine	0.105	D-Glucose	4.5
L-Lysine·HCl	0.146	Phenol Red·Na	0.0159
L-Methionine	0.03	Pyruvic Acid·Na	0.11
L-Phenylalanine	0.066	$NaHCO_3$	3.7
L-Serine	0.042	—	—

Calculations about volumetric energy density and power density of flexible SIB

The detailed calculations about the volumetric energy density and power density of flexible SIB are given as follows:

The volumetric energy density is calculated according to Equation 1,

$$E_{vol} = \frac{C \times V \times m}{v} \quad \text{(Equation 1)}$$

Where E_{vol} is volumetric energy density (Wh cm^{-3}); C is the discharge specific capacity (mAh g^{-1}) of flexible SIB, calculated based on total mass of cathode and anode; V is average discharge voltage; m is the total mass of cathode and anode; v is the volume of the flexible SIB.

The volumetric power density is calculated according to Equation 2,

$$P_{vol} = i_v \times V \quad \text{(Equation 2)}$$

where P_{vol} is volumetric power density (W cm^{-3}); i_v is applied volumetric current density (A cm^{-3}); V is average discharge voltage.

Supplemental References

S1. Zuo, W.H., Wang, C., Li, Y.Y., and Liu, J.P. (2015). Directly grown nanostructured electrodes for high volumetric energy density binder-free hybrid supercapacitors: A case study of CNTs/$Li_4Ti_5O_{12}$. Sci. Rep. *5*, 7780.

S2. Yang, P.H., Xiao, X., Li, Y.Z., Ding, Y., Qiang, P.F., Tan, X.H., Mai, W.J., Lin, Z.Y., Wu, W.Z., Li, T.Q., *et al.* (2013). Hydrogenated ZnO core-shell nanocables for flexible supercapacitors and self-powered systems. ACS Nano *7*, 2617-2626.

S3. Xu, J., Wang, Q.F., Wang, X.W., Xiang, Q.Y., Liang, B., Chen, D., and Shen, G.Z. (2013). Flexible asymmetric supercapacitors based upon Co_9S_8 nanorod//Co_3O_4@RuO_2 nanosheet arrays on carbon cloth. ACS Nano *7*, 5453-5462.

S4. Lu, X.H., Yu, M.H., Zhai, T., Wang, G.M., Xie, S.L., Liu, T.Y., Liang, C.L., Tong, Y.X., and Li, Y. (2013). High energy density asymmetric quasi-solid-state supercapacitor based on porous vanadium nitride nanowire anode. Nano Lett. *13*, 2628-2633.

S5. Lee, J.A., Shin, M.K., Kim, S.H., Cho, H.U., Spinks, G.M., Wallace, G.G., Lima, M.D., Lepro, X., Kozlov, M.E., Baughman, R.H., *et al.* (2013). Ultrafast charge and discharge biscrolled yarn supercapacitors for textiles and microdevices. Nat. Commun. *4*, 1970.

S6. Yang, P.H., Ding, Y., Lin, Z.Y., Chen, Z.W., Li, Y.Z., Qiang, P.F., Ebrahimi, M., Mai, W.J., Wong, C.P., and Wang, Z.L. (2014). Low-cost high-performance solid-state asymmetric supercapacitors based on MnO_2 nanowires and Fe_2O_3 nanotubes. Nano Lett. *14*, 731-736.

S7. Xiao, X., Li, T.Q., Yang, P.H., Gao, Y., Jin, H.Y., Ni, W.J., Zhan, W.H., Zhang, X.H., Cao, Y.Z., Zhong, J.W., *et al.* (2012). Fiber-based all-solid state flexible supercapacitors for self-powered systems. ACS Nano *6,* 9200-9206.

S8. Le, V.T., Kim, H., Ghosh, A., Kim, J., Chang, J., Vu, Q.A., Pham, D.T., Lee, J.H., Kim, S.W., and Lee, Y.H. (2013). Coaxial fiber supercapacitor using all-carbon material electrodes. ACS Nano *7,* 5940-5947.

S9. Tao, J.Y., Liu, N.S., Ma, W.Z., Ding, L.W., Li, L.Y., Su, J., and Gao, Y.H. (2013). Solid-state high performance flexible supercapacitors based on polypyrrole-MnO_2-carbon fiber hybrid structure. Sci. Rep. *3,* 2286.

S10. Yao, B., Yuan, L.Y., Xiao, X., Zhang, J., Qi, Y.Y., Zhou, J., Zhou, J., Hu, B., Chen, W. (2013). Paper-based solid-state supercapacitors with pencil-drawing graphite/polyaniline networks hybrid electrodes. Nano Energy *2,* 1071-1078.